9

Nanostructured thin films and devices based on metallic oxides grown by facile routes

Mostefa Benhaliliba[*1], A. Ayeshamariam[2]

[1]Material Technology Department, Physics Faculty, USTOMB University, BP1505 Oran, Algeria
[2]Research and Development Centre, Bharathiyar University, Coimbatore, 641046, India
[*]Corresponding author

Outline

Introduction

Metallic oxides belong to a wide band gap semiconductor family containing tin oxide (SnO_2), cadmium oxide (CdO) [1-2], indium tin oxide (ITO), indium oxide (In_2O_3) [3-4] and zinc oxide (ZnO) [5-7]. These materials are prepared using techniques such as sol-gel spin coating [8], spray pyrolysis deposition (SPD) [9], hydrothermal route [10], sputtering [11] and colloidal solution route [12]. Sol-gel spin coating and spray pyrolysis deposition techniques have been used in this study because they are nontoxic, low-cost, facile, rapid, unobtrusive, and environmental and have a low processing temperature. Nanoscale metal oxide materials have been attracting much attention because of their unique size- and dimensionality-dependent physical and chemical properties as well as promising applications as key components in micro/nanoscale devices. Nowadays layers of zinc, tin and others metallic oxides become a multifunctional material and the most studied material due to their various properties such as high transmittance in visible range, high reflectivity in the infrared, wide direct band gap around 1.5-3.5 eV, large exciton binding energy at room temperature, and mainly to the huge application areas in microelectronic, solar, photocatalytic and sensors devices. All these encouraged characteristics of the multifunctional materials attract researchers to use them in many applications like solar cells, light emitting diodes [13-14], sensors [15], and field emission device transistors [16]. Nanoscale inorganic materials such as quantum dots (0-dimensional) and 1-dimensional (1D) structures, like nanotubes, nanobelts, and nanowires have attracted interest of many researchers' attention within the last decade [17-20]. This chapter provides a detailed overview of nanostructured oxides films such as ZnO, Sn_2O, CuO and CdO and provides a guidance study to researchers working in the nanostructured films and devices based on oxides. Beside, semiconducting oxide sensors have been studied intensively due to their sensitivity to a large number of gases. Due to their difference in morphology and roughness, the coated films exhibit difference in optical and photoluminescent properties. Moreover, such coated layers present difference in optical and electrical parameters due to their different crystalline structure and optical bandgaps. The nanostructure of oxides growing by a simple and low-cost coating routes namely jet nebulizer spray pyrolysis, spin coating and sputtering techniques are investigated. The as-grown oxides onto corning glass, ITO and silicon substrates are analyzed by X-ray pattern, UV-Vis-IR spectrophotometer, atomic force microscope (AFM), and room temperature photoluminescence set up. The electronic characteristics are carried out using Keithley source meter in room temperature, under dark and light conditions. The variation of the sensitivity are measured for SnO_2 layer coated over In_2O_3 using the set-up constructed using a vacuum coating unit. Several perspectives on future research on metallic oxide nanostructures are emphasized and also provided.

Thin films and devices based on metallic oxides achievement

Polycrystalline structure of layers based on oxides

Polycrystalline structure of as-grown layers based on oxide is shown in figures 9.1-9.3. The (002) orientation, for the pure and In doped ZnO (IZO) layers is observed. X-rays diffraction analysis of IZO films versus pure ZnO in the 20-100° range of angle 2θ is shown in figure 9.1. At high substrate temperature of 400°C, the film exhibits only a (002) reflection. All cases present a (002) plane with different magnitudes, but the (101) and (103) orientations are only observed in pure and IZO

prepared at substrate temperature lower than 400°C. Among the standard ZnO reflections, the (002), (101), (102), (103) and (112) planes have been detected in the majority of films except the IZO films grown @400°C, which exhibits only the strong (002) orientation. However, all the as-grown IZO films demonstrate a polycrystalline nature, fitting well with the hexagonal ZnO wurtzite-type structure. No phases corresponding to In_2O_3 nor to other zinc indium compounds are detected. According to the standard card N^{er} 36-1451-of ZnO polycrystalline structure, the (002) (2θ ~34.42°) plane is seen in all cases with different intensities. Although the (002) orientation, for the pure and doped ZnO film is observed, the (101) plane varies decreasingly from the undoped to the doped films.

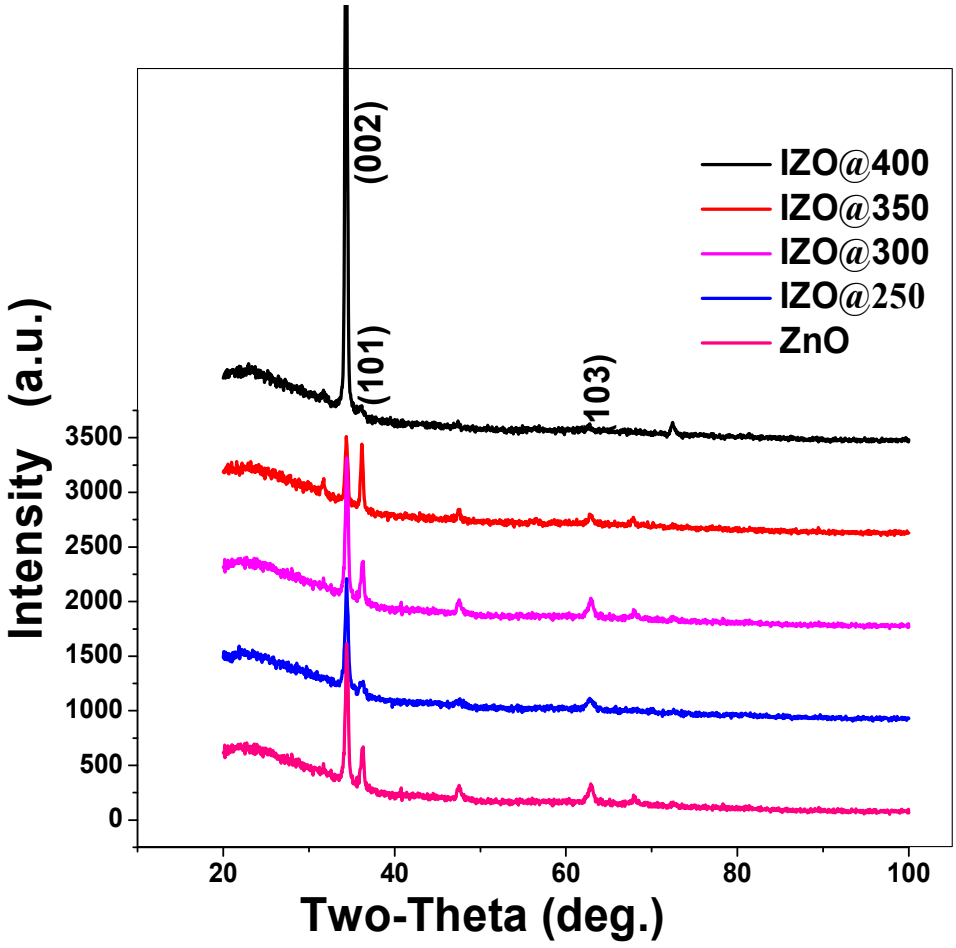

FIGURE 9.1
X-rays pattern of pure and indium (IZO) doped ZnO grown by ultrasonic nebulizer spray , Bragg angle ranges within 20°-100°, indexation of main peaks is shown. The IZO films are prepared at 250-300-350 and 400°C

The figure 9.2 shows the XRD pattern of the pure ZnO and CeO_2 nano compounds. There are number of intensive peaks are observed from (111), (002), (200) and (112) planes for CeO_2 and from (100), (101), (102), (110) and (103) for ZnO. These signals confirm the simple cubic and

hexagonal lattice form of pure ZnO and CeO_2 nano compounds respectively. The corresponding lattice constants are a=b=c=5.411 Å for cubic and a=b=3.249 Å; c=5.206 Å for hexagonal structure.

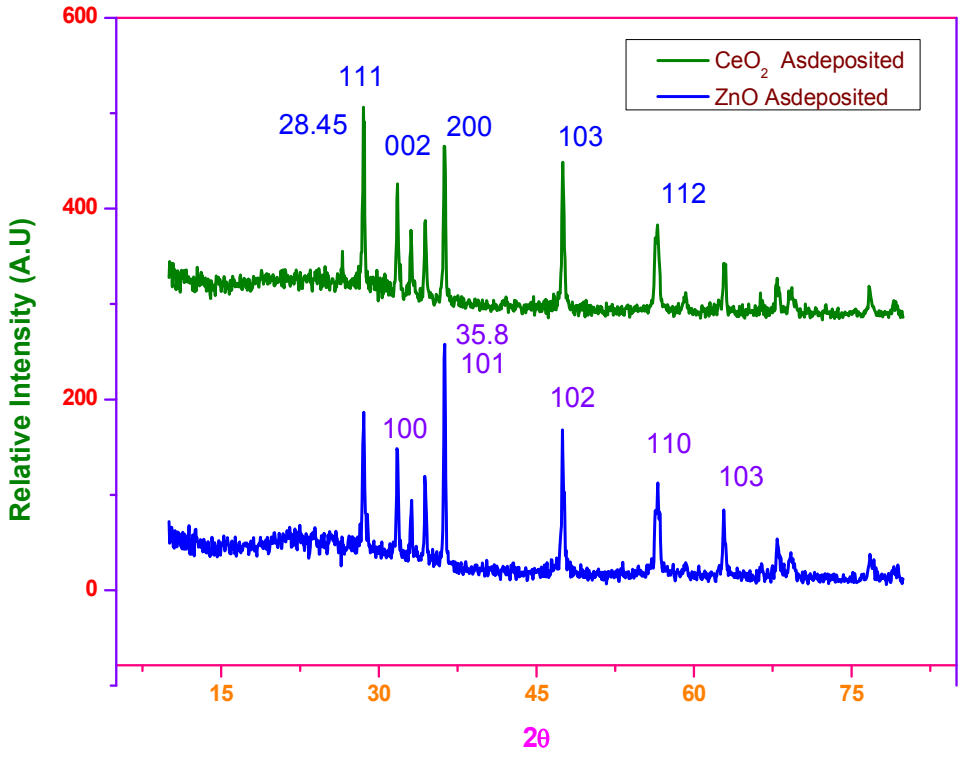

FIGURE 9.2
XRD analysis of CeO_2 and ZnO layers via spin-coating sol–gel method

The as-grown films are identified as polycrystalline SnO_2 with a tetragonal crystal structure and preferred orientation along the (200) plane as shown in figure 9.3. The as-deposited layers exhibit the tin oxide (SnO_2) structure and no other phase than structure of SnO_2 is detected, as reports the JCPDS card (N° 72-1147) data of SnO_2. Pure tin oxide (TO) film exhibits intense peak at $2\vartheta \sim 37.8°$. The main strong peaks are (200), (211) and (101) as evidenced in figure 9.3 which identify the tetragonal structure; the weak peaks ($2\theta>54°$) demonstrate the presence of SnO_2 orthorhombic structure. Besides, the peak (200) is very intense in the case of pure TO, Al level doping reduces it. While (211) orientation increases with Al doping level mainly for 1.5 % and 8.5 % sprayed films. Furthermore, (101) direction decreases with an increase of Al doping content, whereas the peaks of orthorhombic TO cases become insignificant in the doped samples as seen in figure 9.3. Overall, these peaks present roughly a peak broadening (FWMH increases) which leads us to report on nanostructures formation. This report is confirmed by the slight grain sizes of as- grown TO samples (see table 9.1). The increase of Al doping level leads to decrease in crystallinity degree, this result is also reported in literature [21].

TABLE 9.1
Structural (grain size according to (200) plane, lattice parameters *a*, Δa, c, Δc, the strain ε_{zz} along c orientation, unit cell volume V, ΔV/V), optical (T at 550 nm), morphological (RMS, grain size by AFM measurement) parameters of pure and Al doped tin oxide Al:SnO_2 thin films produced by spray pyrolysis onto glass at 300 °C [22]

Al level (%)	Grain size (XRD) (nm)	Lattice constants (Å)				ε_{zz} (%)	V (Å^3)	ΔV/V (%)	T (550nm)	RMS (nm)	Grain size (AFM) (nm)
		a	Δ*a*	*C*	Δ*c*						
0	20.98	4.745	0.008	3.201	0.016	0.502	72.104	90.28	88.252	10.41	90.28
1	26.81	4.718	-0.019	3.218	0.033	1.036	71.660	149.31	75.475	19.09	149.31
1.5	21.61	4.712	-0.024	3.212	0.027	0.848	71.342	41.67	80.701	15.82	41.67
3	19.83	4.707	-0.030	3.219	0.034	1.067	71.343	27.78	77.439	10.84	27.78
8.5	21.57	4.715	-0.022	3.211	0.026	0.816	71.394	101.56	77.435	11.52	101.56

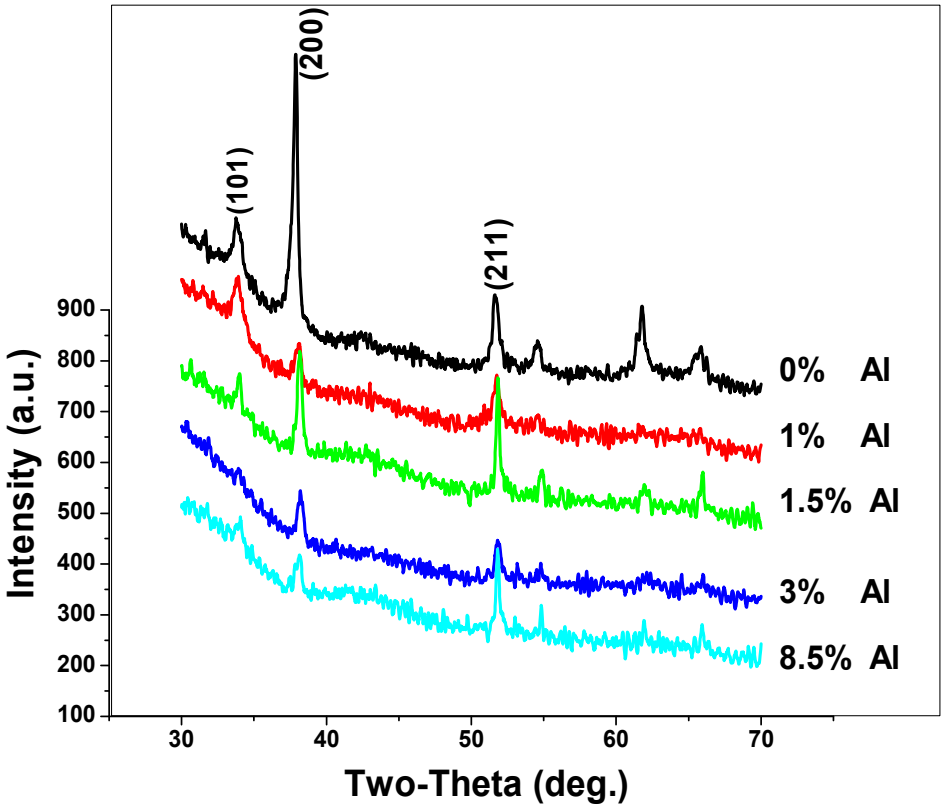

FIGURE 9.3
X-rays pattern of pure and aluminum doped SnO_2 grown by ultrasonic spray nebulizer spray, Bragg angle ranges within 30°-70°. Al doping level varies within 1-8.5 % range

The high transparent coated layers based on oxides

The optical properties of ZnO, SnO_2 and CuO and their related doped compounds are carried out using an accurate UV-VIS-IR spectrophotometer. As shown in figures 9.4-9.6, the high transmittance (> 80%) in visible and IR bands is distinguished.

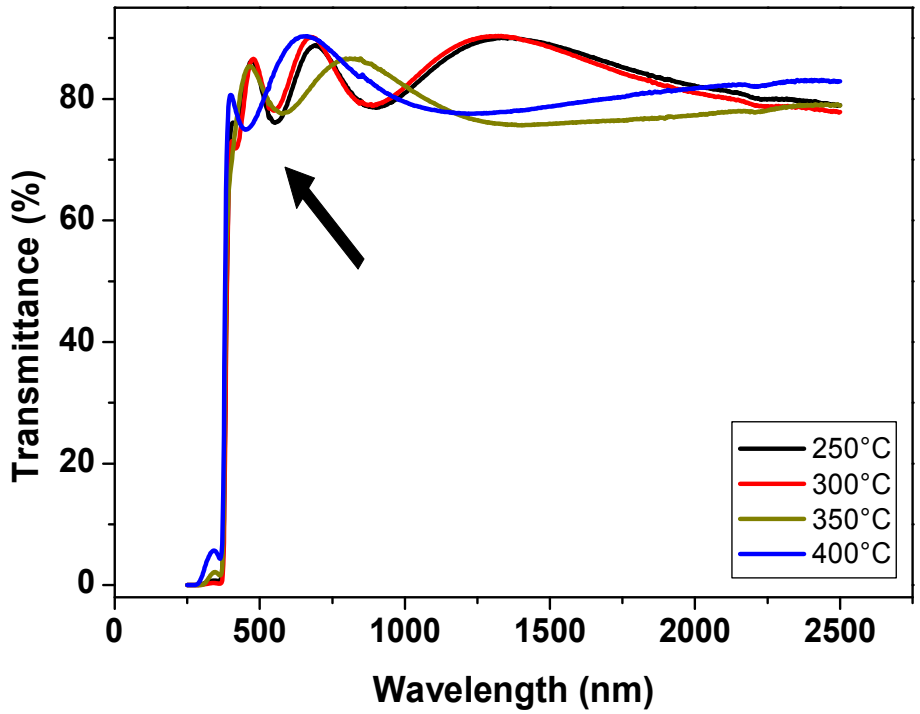

FIGURE 9.4
The UV-VIS-IR transmittance versus photon wavelength of ZnO films which have grown within the 250-400 °C substrate temperature range

A sharp increase of transmittance from UV (<400 nm) to visible band (400<λ<800 nm) is detected and several oscillations in the Vis-IR ranges are observed as shown by arrow in figures 9.4-9.6.
The pure tin oxide presents only one oscillation in visible range of 88.25 %, at 550 nm, followed by a slight decay and an increase in infrared spectrum from the wavelength of 1200 nm. In the visible band, the transmittance of sample A (see table 9.2 below) reached a maximum of 81% around a wavelength of 600 nm, followed by a decay of about 5% from 600 nm to the visible band edge. A second maximum of transmittance is obtained in the IR spectrum and found to be 89% and the transmittance is also decreased rapidly by 15% in medium and far-infrared band. Sample B exhibited another variation of transmittance. This latter increased rapidly in UV–VIS shaped two oscillations and highest transmittance is around 88%, and then decreased rapidly by 38% in the VIS–IR band. High transmittance (90%) of SnO2 is obtained by Moure-Flores [23]. The structural parameters of sprayed ZnO and IZO layers are listed in table 9.3. A biggest grain size of 221 nm is reached for the case of pure ZnO film produced @ 350 °C while the smallest one (17 nm) is obtained for IZO layer @ 250 °C.

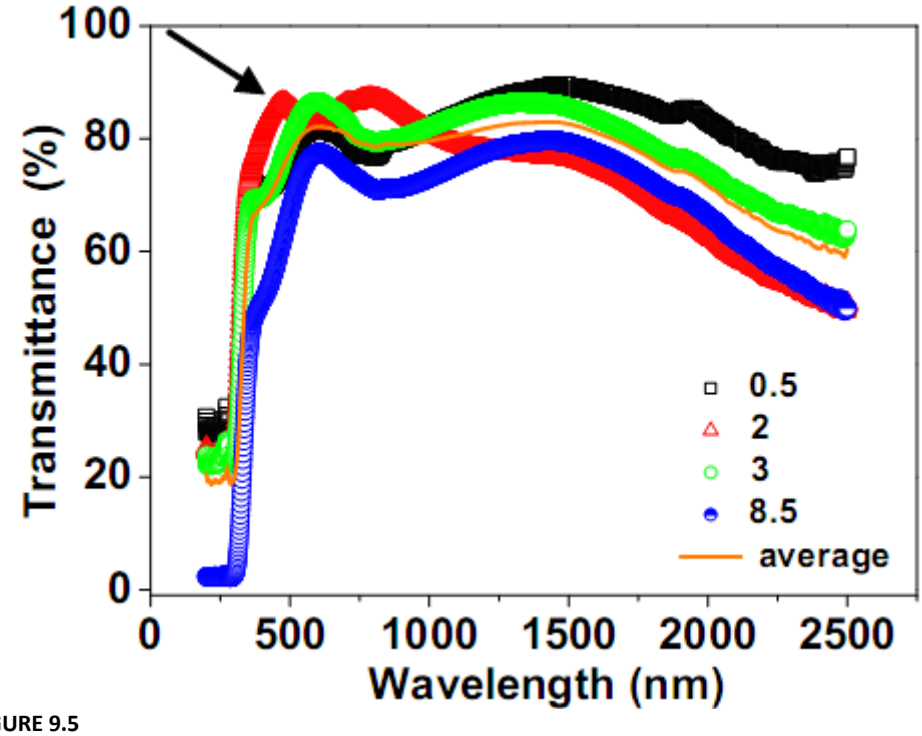

FIGURE 9.5
The UV-VIS-IR transmittance dependence on the photon wavelength of sprayed Al:SnO_2 films produced at 300 °C. Black arrow showed the oscillations and average curve is sketched (brown solid line). (A: 0.5, B: 2, C: 3, D: 8.5 %Al doped SnO_2)

TABLE 9.2
Grain size by X-rays pattern, transmittance at wavelength of 550 nm, Transmittance at wavelength of 550 nm, optical band gap, thickness of films and figure of merit, root mean square roughness and RMS (nm) of sprayed Al:SnO_2 grown onto ITO glass substrate at 300 °C (sample A:0.5, B:2, C:3 and D:8.5 %) [1]

Samples (Al %)	Grain size by X-rays pattern (nm) along (211) plane	T(550 nm) (%)	E_g(eV)	Thick (nm)	Figure of Merit ($x10^{-3}\ \Omega^{-1}$)	RMS (nm)
A:0.5	11.4	80.74	3.46	231.5	12	12.52
B:2	11.3	83.51	3.55	297.6	0.1	209.63
C:3	8.1	85.15	3.45	238.1	49	25.55
D:8.5	42.6	74.85	3.25	232.7	$7x\ 10^{-4}$	348.70

The optical properties such as transmittance and optical band gap from absorption data are determined using a spectrophotometer in the range between 200 nm and 2500 nm as sketched in figure 9.6. In UV band, the sample annealed @ 250°C exhibits a strong transmittance of 33%

compared to the samples heated at high post-annealing temperatures and then sharply decreases as wavelength shifts to visible edge and increases rapidly to reach a peak of 76% in the infrared range @ 826 nm (1.5 eV) (showed by arrow in figure 9.6) and exhibits an edge around 520 nm. The transmittance changes from 74% to 80% in the IR band, this property will give the sputtered CuO special applications in micro-optoelectronic devices. Furthermore, the absorbance increases in the UV region with increasing the annealing temperature. The absorption edge which occurs around 530 nm might due to the Cu_2O phase which is formed at lower post-annealing temperature and vanishes to higher ones. This latter detail is confirmed by XRD pattern as indicated in table 9.1. As seen in figure 9.6, curve of transmittance reaches a high point of 80% in the 450-830 nm wavelength range. The absorption coefficient is expressed as follows [1],

$$\alpha = -\frac{\ln T}{t} \quad (1)$$

Where t is the thickness of films ranged between 120 and 255 nm, T is the transmittance and α is the absorption coefficient.
A post-annealing effect on the sputtered CuO/Si device properties is described in table 9.4.

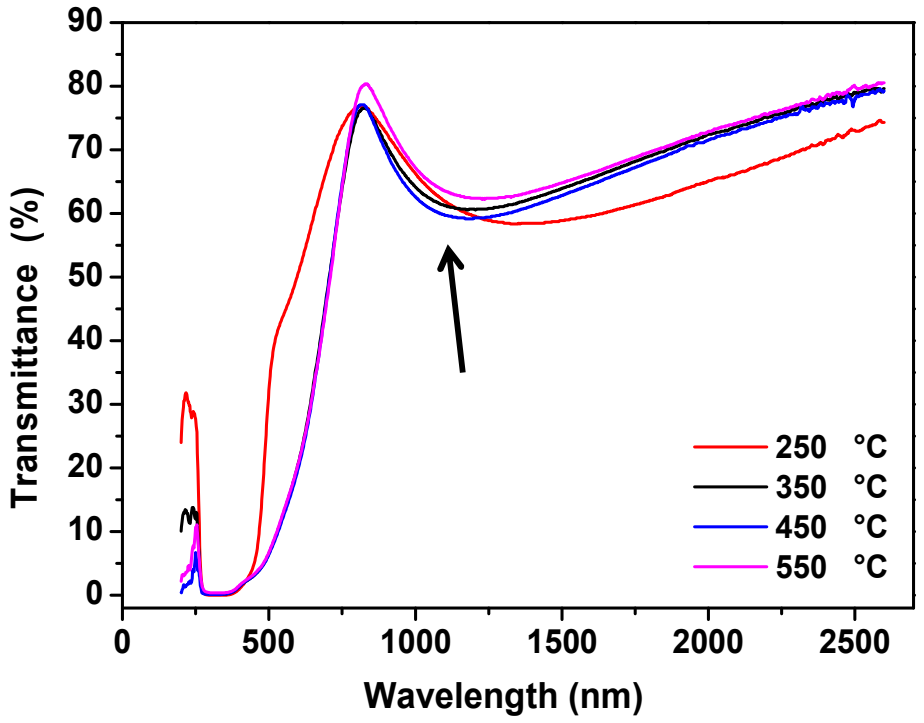

FIGURE 9.6
Transmittance plot vs. photon wavelength of sputtered CuO layers post-annealed at several temperatures (250-550°C)

The performed nanostructures of films based on oxides

The area scanned AFM surface studies show nanostructures occurrence with different sizes, shapes and orientations. The formed nanograins look like mountains. As shown in figure 9.7, the films growth of Al-doped ZnO onto glass substrate follows the z-axis direction; the average height is about 1 µm. The surface is composed with wrinkled long grains. The (10µmx10µm) scanned 3D-view of Cd-doped ZnO layer exhibits a fiber structure where the fibers grow along z-axis direction as seen in figure 9.8. While the Sn doped ZnO films presents tip topography along the z-direction up to 180 nm. Overall, the surface is homogenous with a few avoids, some grains seem to tip-mountain with a broadened head and the estimated average grain size is around 1µm as shown in figure 9.9. Prepared with a same coating process and speed of 1200 rounds per minute (rpm), 2% Cu-doped CdO films surface exhibits a tip texture morphology as seen in figure 9.10. According to z-axis orientation, the grains are separated with different heights (max. height=275.7 nm) as seen in figure 9.10, the height of grains increased and the similar texture is observed for the 3% Cu doped CdO layers (see fig. 9.11).

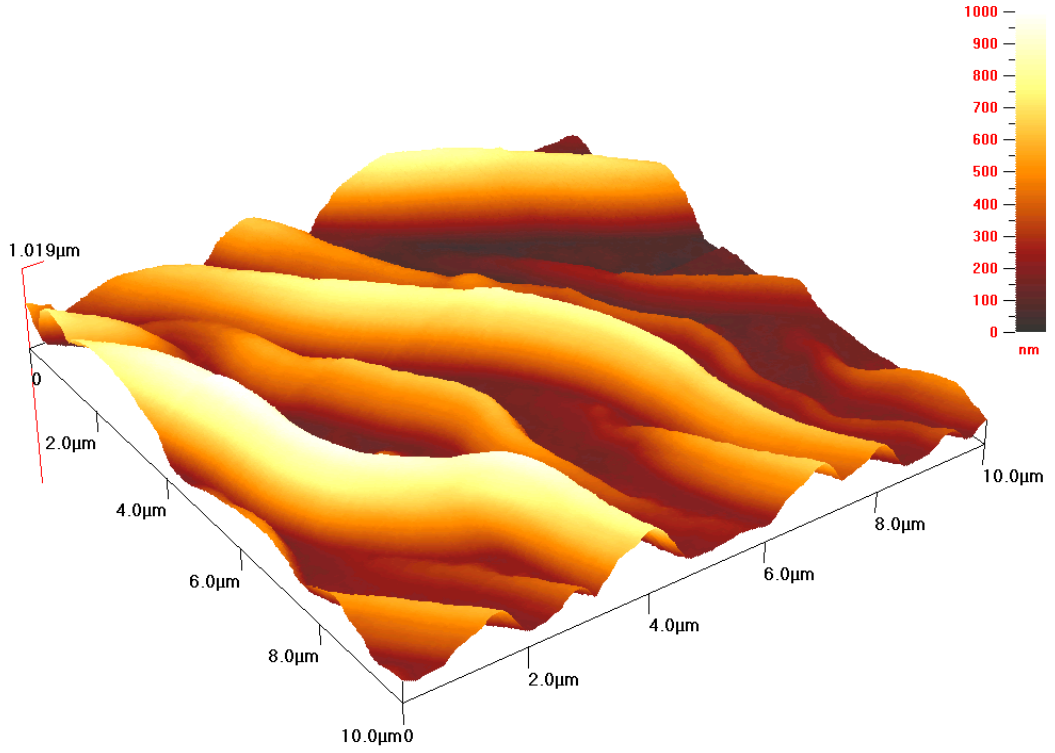

FIGURE 9.7
3% Al doped ZnO onto glass substrate prepared by sol-gel spin coating process @ 1200 rpm

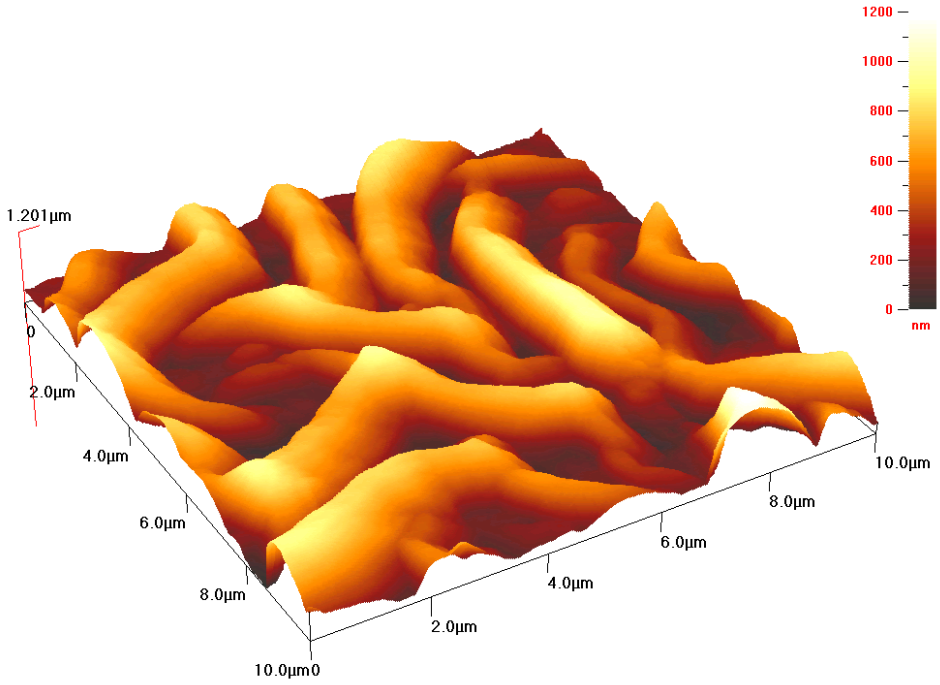

FIGURE 9.8
3% Cd doped ZnO onto glass substrate prepared by sol-gel spin coating process @1200 rpm

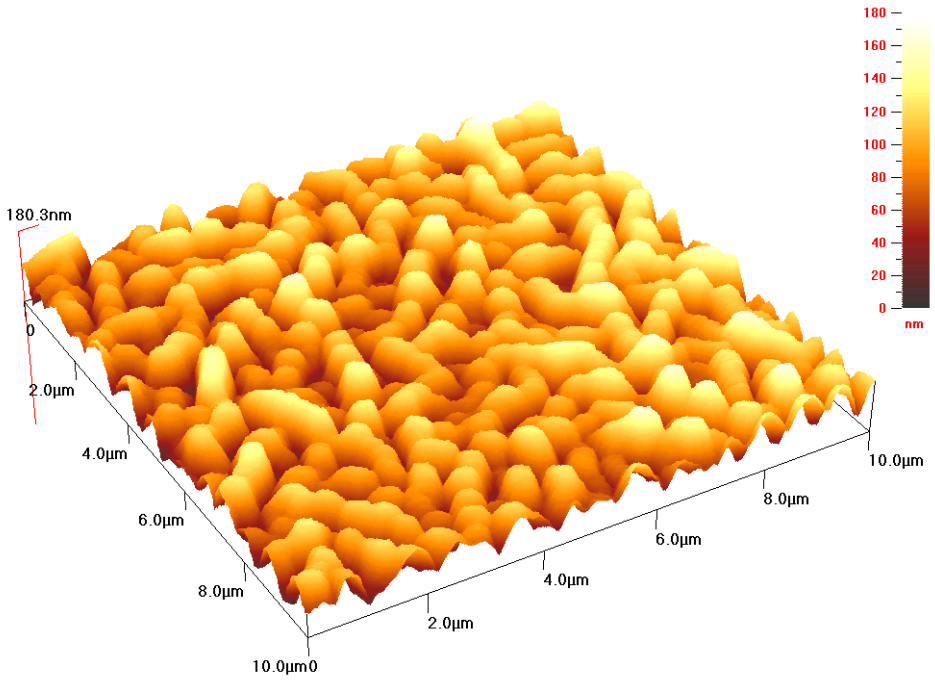

FIGURE 9.9
2% Sn doped ZnO onto glass substrate prepared by sol-gel spin coating process

Coated pure CdO films present a grain size of 75 nm, while the Cu doping increases the grain size up to 208 nm.

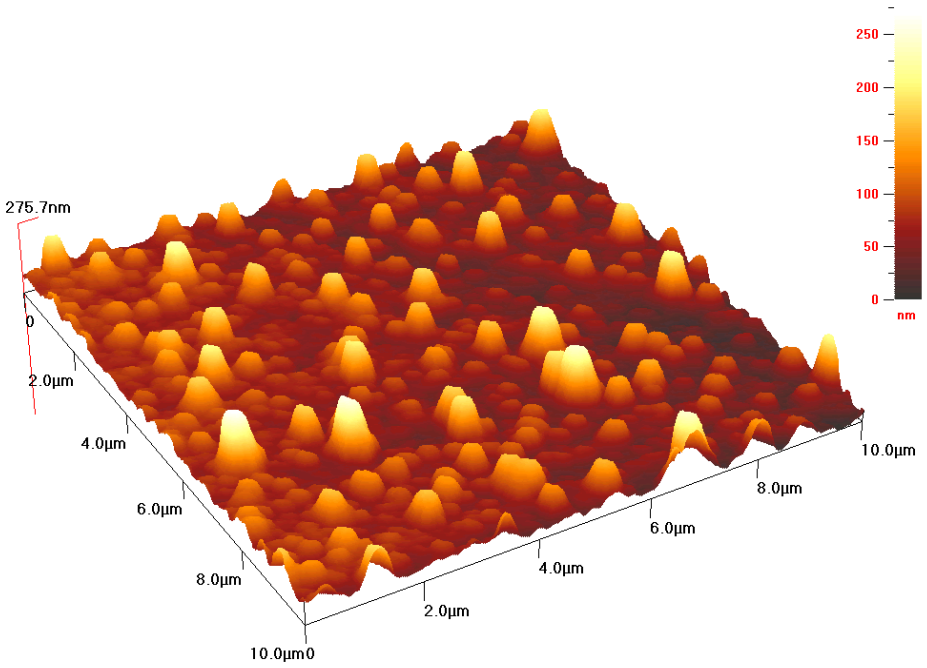

FIGURE 9.10
2% Cu-doped CdO film produced on glass substrate @ 1200 rpm by sol-gel spin coating process

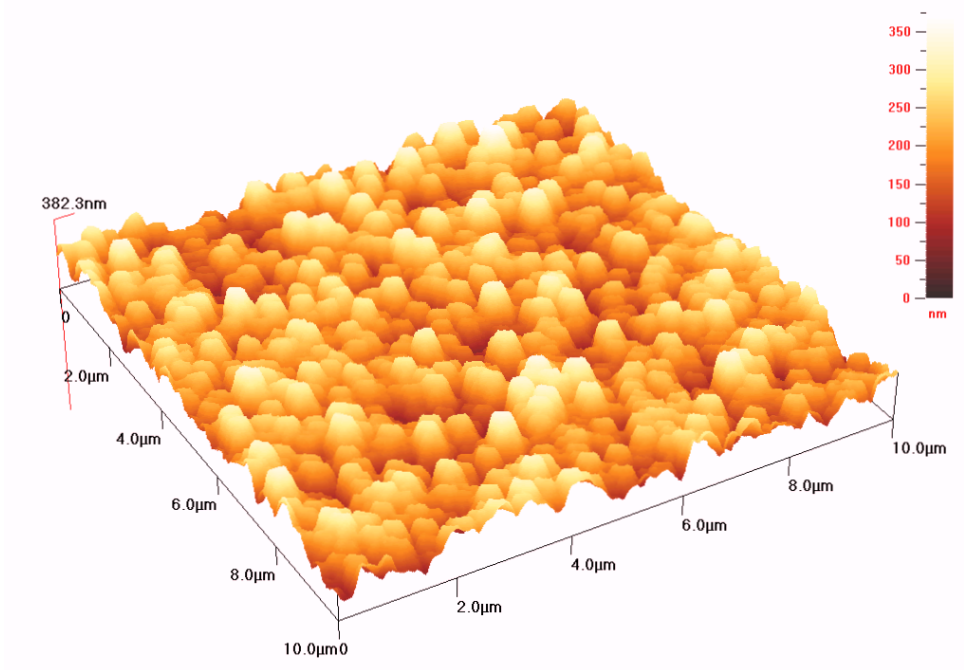

FIGURE 9.11
3% Cu-doped CdO film produced on glass substrate @ 1200 rpm by sol-gel spin coating process

Nanostructures of Al-doped SnO_2 are successfully produced onto ITO-coated glass via spray pyrolysis method at a constant substrate temperature of 300 °C. To characterize the topography and confirm the nanostructure property, we performed AFM observations on the Al-doped SnO_2 films. Figure 9.12 shows the 3D-AFM views of 2 % Al-doped SnO_2 film produced onto ITO coated glass substrate by spray pyrolysis technique. The films of Al:SnO_2 revealed roughly a homogenous surface consisting of crystallites. The crystallites are grown from the inner towards the surface. The AFM observation showed a large amount of grain agglomeration that looked like assembled nanofoam with few voids. The average size is evaluated at 65 nm, and the root mean square roughness (RMS) of films is of 210 nm. In addition, these nanograins are concentrated with no well boundaries. Similar nanostructures SnO_2 morphology is found in literature [24]. It is confirmed that Al doping level influenced grain structures as sketched in figures 9.12-9.13. Nanograin-like assembled tips are shaped in the 0.5% Al-doped tin oxide film as observed in figure 9.13. Overall, its surface is homogenous and grains have different sizes, look like tips with an almost circular base and a very sharp peak. Moreover, nanotips are smooth (RMS ~12.5 nm) compared to those obtained from other samples as listed in table 9.2, and grown along the z-axis. The nanotips grow side by side with a high surface density (number of nanotips / µm²) leaving almost no voids. These configurations are in well agreement with those obtained by Chacko [24].

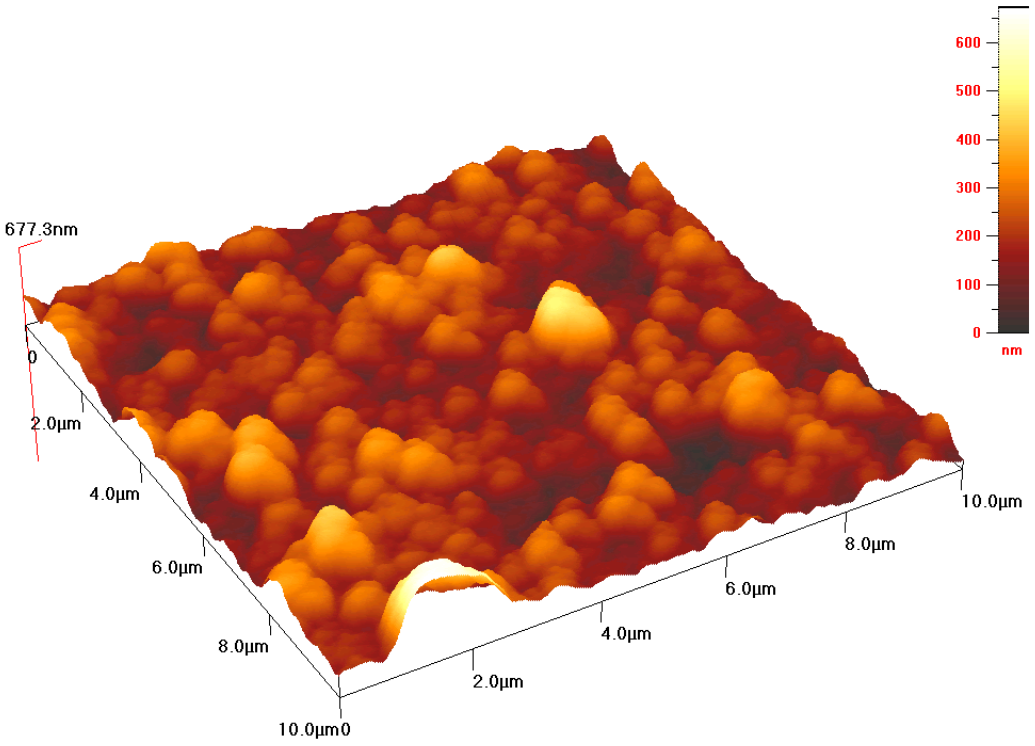

FIGURE 9.12
2 % Al-doped SnO_2 film produced on ITO glass substrate by spray pyrolysis technique

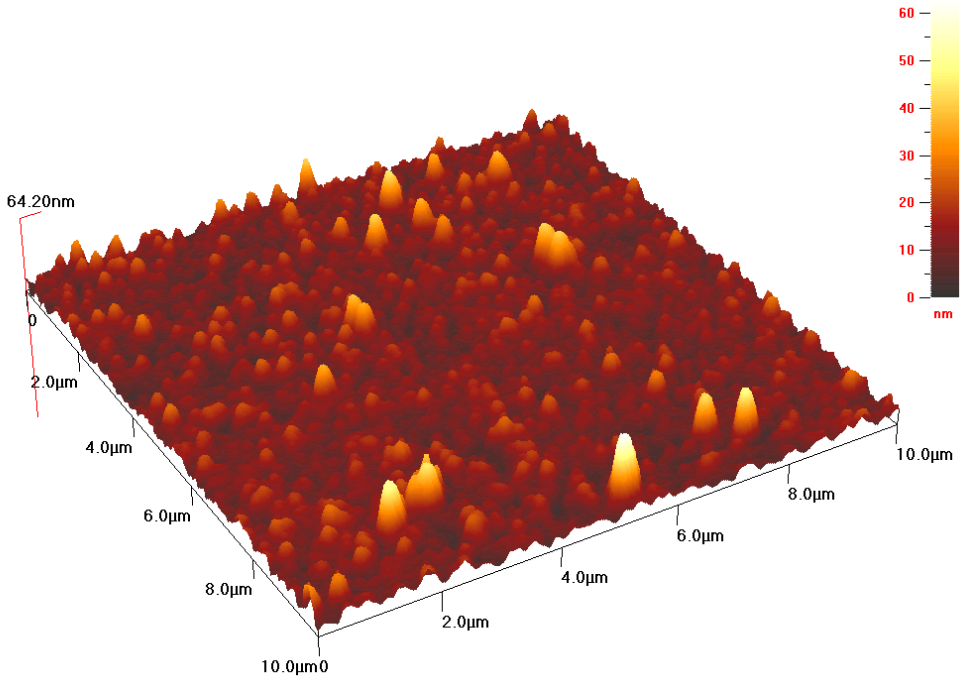

FIGURE 9.13
0.5 % Al-doped SnO_2 film produced on ITO glass substrate by spray pyrolysis technique

The 3D Atomic force microscopy image of the coated over In_2O_3: SnO_2 films deposited in the concentrations ratio of 50:50. AFM results show spherical grains in all the films with varied smoothness as sketched in figure 9.14. The grain size of In_2O_3: SnO_2 films deposited at 75:25 concentration (not shown here) in each at 20 min time of deposition is smaller than that of the films deposited at the concentrations of 70:30 at 20 min (not shown here), which is also confirmed in XRD result. However, at 20 min time of deposition, of different concentrations the size distribution is non–uniform. Whereas, in the film deposited at 20 min time of deposition at 75:25 uniform grains are observed. The AFM image gives the RMS roughness value, which will be indicating the film surface smoothness quantitatively. The RMS roughness value is of 3.05 nm.

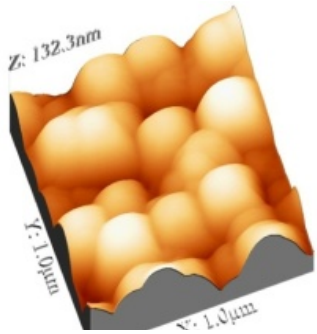

FIGURE 9.14
The Atomic force microscope (AFM) topography image for ITO films deposited for 25, 30 and 50 % SnO_2 doping level. The foam-like structures called “aero gel” are observed

TABLE 9.3
The (hkl) planes, the grain size (G), the dislocation density (δ), the textural coefficient (TC), lattice parameters (a, c) and strain parameter (εzz) of sprayed ZnO and indium doped ZnO (IZO) thin films onto glass substrates [25]

Sample	(hkl) Planes	G (nm)	δ ($x\ 10^{-5} nm^{-2}$)	TC	Lattice parameters (Å)	ε_{zz}
ZnO@350°C	(002) (101) (102)	39 94 221	65 11 2	1.56 0.58 0.86	a=3.290 c=5.200	$3.8x\ 10^{-2}$
IZO@250°C	(002) (101)	24 17.5	$1.7\ x10^{2}$ $3.2\ x10^{2}$	1.53 0.47	a=3.006 c=5.207	$1.9x\ 10^{-2}$
IZO@300°C	(002) (101)	28 22	$1.2x\ 10^{2}$ $1.9\ x10^{2}$	1.42 0.58	a=2.440 c=5.207	$1.9x\ 10^{-2}$
IZO@350°C	(002) (101)	24 24	$1.7x\ 10^{2}$ $1.6x\ 10^{2}$	0.75 1.25	a=3.252 c=5.214	0.15
IZO@400°C	(002)	30.5	$1.07x\ 10^{2}$	1.92	c=5.215	0.17

The photoluminescent layers based on metallic oxides

The photoluminescence (PL) spectra of Zn doped CeO_2 is examined in the range of 350 -550 nm by PL spectrophotometer deposited at room and annealed at 350ºC temperatures. The CeO_2 is a type of wide band gap semiconductor compound. The spin-orbit interaction in the three unequal crystal axes intersecting at oblique angles. The PL spectra of ZnO-CeO_2 and its annealed thin films on glass substrate are shown in Figure 9.15. The PL spectrum showed multiple modulated signal bands in the region of 350- 550 nm in which a peak is assigned to edge green region (520 nm) and a less intense in the blue region (490 nm). The spectral peak intensity of compound as deposited is less than at 350 °C. These results showed that, the peak at 390 nm is the band-edge free exciton luminescence, while the peak at 490 nm is the bound exciton luminescence [26]. The PL emission spectra is caused by the recombination of excited electron-hole pairs, so moderate PL intensity indicates lower recombination of the electron-hole pairs, which may result in significant optoelectronic property [27-28] and better photocatalytic properties. In this case, the PL spectrum is very much blue shifted which is purely due to the doping of Zn on CeO. In addition to that, this result is confirmed the nano crystalline nature of present material. The deep states in nano crystalline materials are mainly associated with stoichiometric defects, dangling bonds or external added atoms such as oxygen. But in this case the impurity ZnO is added with the compounds which also support this process. The PL spectrum of the present nano compound reveals that, a peak shift of CeO_2 emission upon ZnO doping which are due to the increment of oxygen defects localized between the Ce^{4F} and O^{2p} energy levels. This view is validated and makes good agreement with previous work [29].

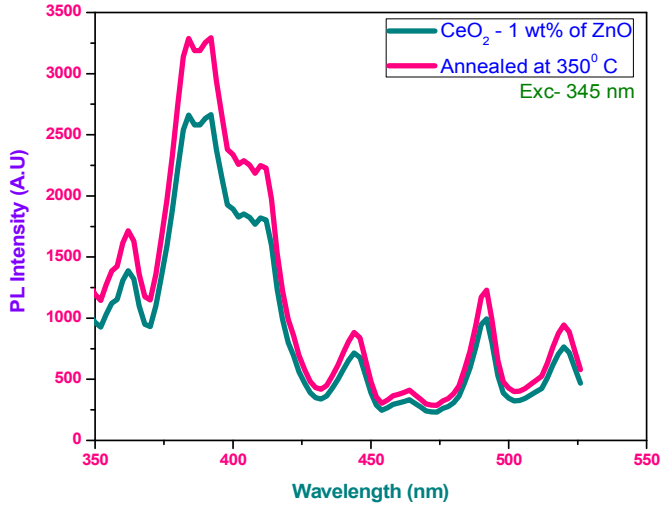

FIGURE 9.15
Photoluminescence plotting of CeO_2 doped with 1% of ZnO at room temperature and annealed at 350º C

The analysis of photoluminescence (PL) spectroscopy at room temperature of spin coated CdO films reveals various peaks as shown in figure 9.16. We use the photoluminescence spectroscopy to determine the band gap of semiconductors since the most common radiative transition in the semiconductor occur between states at the bottom of the conduction band and the top of the valance band. The strong ones are found at 2.11 (right), 2.30, 2.32, 2.44, 2.47, 2.58 and 2.80 (left) eV. PL behaviour shows strong VIS emission around 440 nm (left peak) and 585 nm (right peak) which correspond to violet and orange region of electromagnetic spectrum respectively. The intense emission ~ 442 nm might be attributed to the combination of the electrons from the conduction band and holes from the valence band. Weak peaks are situated in green region from 490 nm (2.53 eV) to 570nm (2.17eV) which are ascribed to defects centers as indicated in figure 9.16.

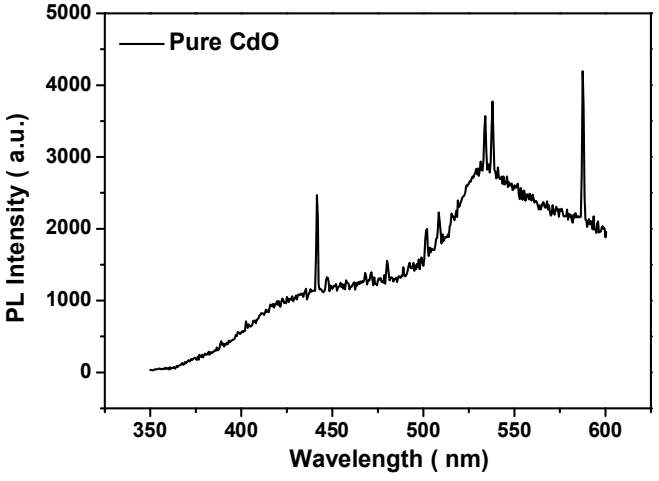

FIGURE 9.16
Photoluminescence behavior against photon wavelength (range 300-650 nm) of pure CdO layers deposited by spin coating process

The dependence of photoluminescence on photon wavelength of ITO films grown by e-beam evaporation (EBE) technique [30] for 25, 30 and 50 % SnO_2 doping level is observed in figure 9.17. A photoluminescence spectrometer consists of two optical system, one for excitation and other for the photoluminescence emission, and each system include a monochromator. The emission line at 3.827 eV has two features: (i) Relative intensity decreases rapidly with increasing intensity and wavelength. (ii) The obvious energy shift is observed with increasing intensity. This spectrum is dominated by the excitonic transition that now has shifted to 3.85 eV.

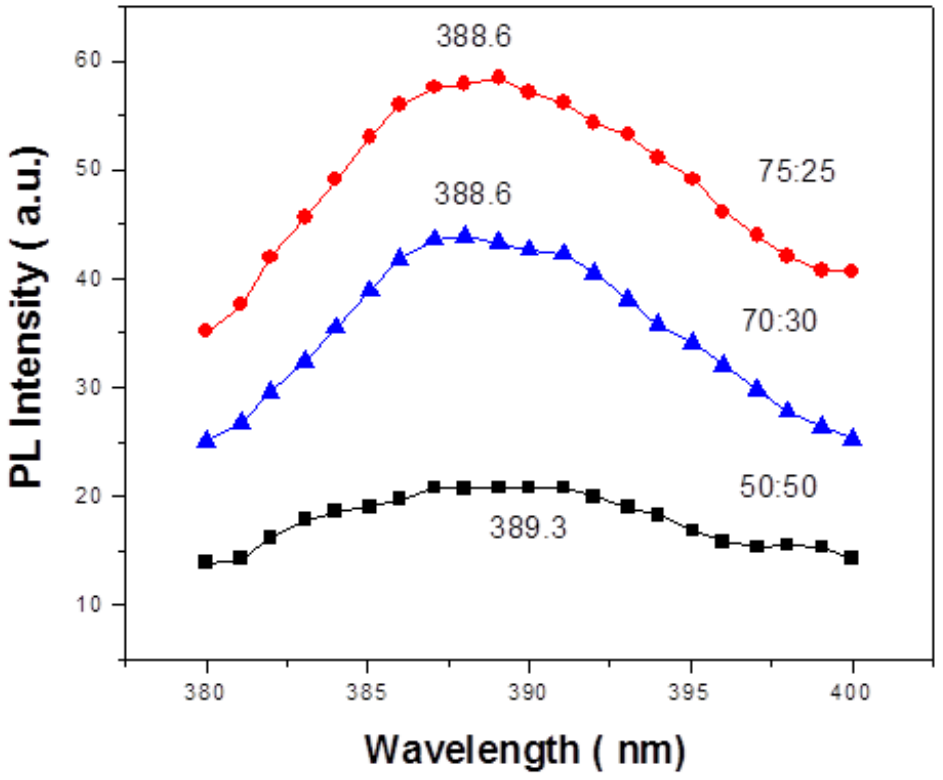

FIGURE 9.17
The dependence of photoluminescence on photon wavelength of ITO films grown by JNS technique for 25, 30 and 50 % SnO_2 doping level

Investigation of electronic devices properties

Deposited onto silicon substrate, metallic oxide like ZnO, SnO_2 and CuO can be a good candidate of schottky diodes. Such oxides are a part in the fabrication of Ag/SnO_2:In/Si/Au Al /ZnO/pSi/Al, Ag/p-CuO/n-Si/Au Schottky diode structures as shown in figure 9.18. The exponential profile of the forward current-voltage characteristics depends strongly on the property of active material used for diode. It is given in terms of voltage and temperature as follows [31-32];

$$I = I_0 \exp(\frac{q(V - IR_s)}{nkT}) \quad (2)$$

The ideality factor of the as-fabricated diode is then given from the following expression [31-32],

$$n = \frac{q}{kT}\frac{dV}{d\ln(I)} \qquad (3)$$

Where k is Boltzmann constant (1.38 10^{-23} J/K), T is the absolute temperature (300 K) and q is the electron charge (1.6 10^{-19} C) [31]. The parameter n is equal to unity in the ideal diode case but for our as-fabricated device it is greater than 1 due to interface density and series resistance. Using the eqn. (3), we determine the ideality factor of metallic oxide/Si contacts Schottky diode from the slope of the linear part of the bias forward ln I–V. The ideality factor n is very important parameter that decide the amount of contribution of tunneling on the recombination process and the change of performance of the device [32], besides high values of ideality factor can be attributed to the presence of the interfacial layer, a wide distribution of the low-Schottky barrier height (SBH) patches (or barrier inhomogeneities), series resistance and therefore, to the bias voltage dependence of SBH.

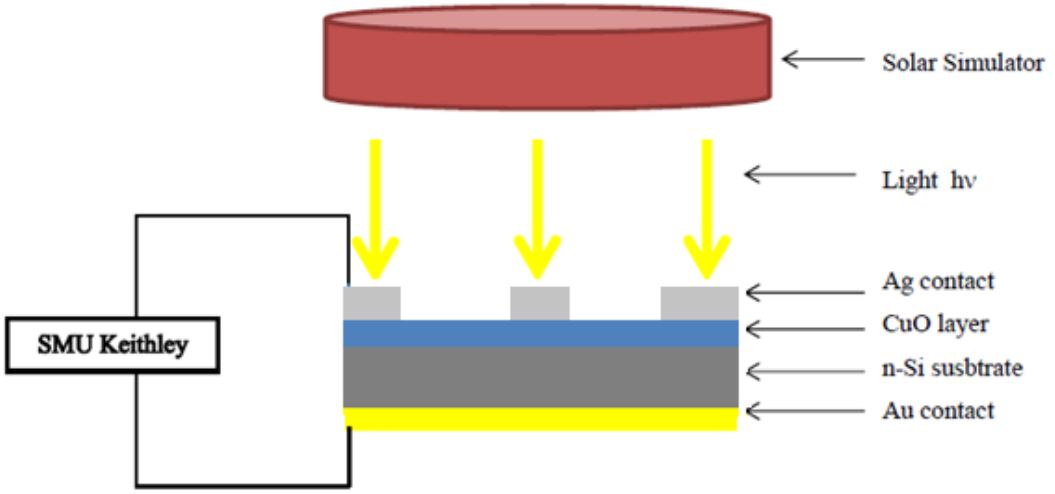

FIGURE 9.18
A cross section schematic of the Ag/p-CuO/n-Si/Au Schottky diode structure

Based upon the best crystalline structure, the higher transmittance, the lower band gap and the best surface morphology, the sample heated at 550°C is selected to fabricate the device. The fabrication and electrical characterization of Ag/p-CuO/n-Si inorganic diode has been investigated. Based on the electrical measurement of current versus bias voltage in dark conditions we extract the parameters such as barrier height, ideality factor, saturation current, series resistance and rectifying factor. Figure 9.19 shows the semi log I-V characteristics of the Ag/p-CuO/n-Si heterojunction in the dark and illuminated. In light condition, the 150 watts correspond to 100 mW/cm^2 (1.5 AM). As can be seen from the plot that illuminated reverse current is larger than that of under dark. This indicates that under illumination electron-hole pairs are produced in p-CuO/n-Si junction generating then a photocurrent. The open circuit voltage (V_{oc}) and the short circuit current (I_{sc}) of the as- fabricated heterojunction are found to be 290 mV and 5.5×10^{-4} A respectively. V_{oc} and I_{sc} values are low causing degrade the conversion efficiency. Moreover, the sputtered device

Ag/CuO/Si/Au exhibits a non-ideal behavior because n is greater than unity (n=3.5). By Norde method [33] the barrier height and the series resistance are extracted and found to be 0.96 V and 86.6 Ω respectively [11].

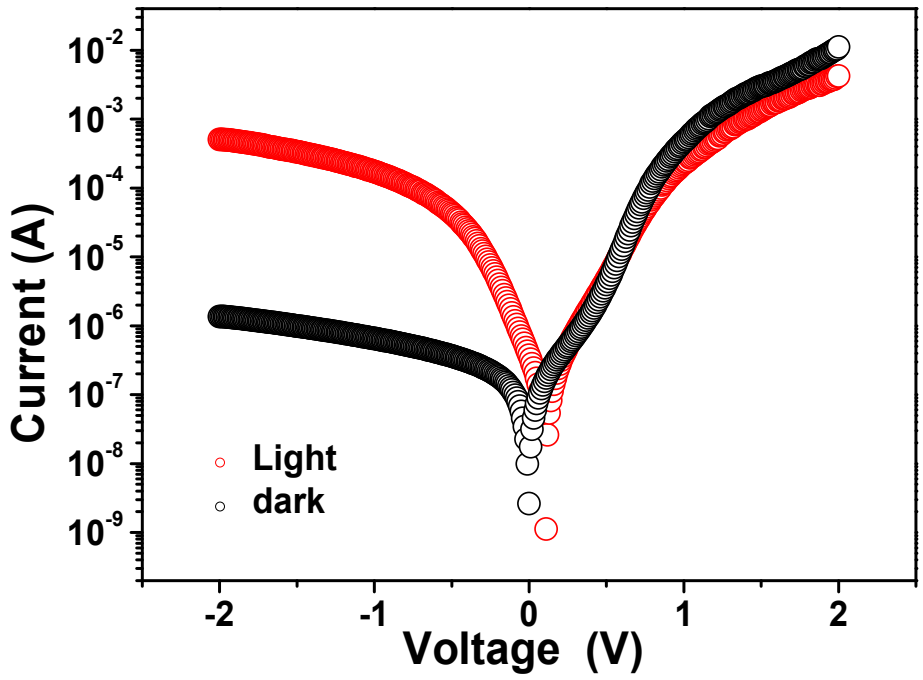

FIGURE 9.19
LogI-V plotting in dark and illumination conditions of Ag/p-CuO/n-Si heterojunction

TABLE 9.4
Annealing temperature, film thickness, carrier concentration, resistivity and mobility of sputtered p-CuO/n-Si layer [11]

Sample	Annealing Temperature (°C)	Film thickness (nm)	Carrier Concentration ($x10^{17}$ cm^{-3})	Resistivity (Ω.cm)	Mobility (cm^2/ Vs)	Conductivity type	Conductivity (10^{-3} Ω.cm)$^{-1}$
1	250	254	0.46	135.2	0.92	P	7.39
2	350	222	7.48	24.56	0.34	P	40.7
3	450	183	11.10	14.91	0.38	P	67.1
4	550	122	45.83	21.81	0.06	p	45.8

Under dark, the Al/ZnO/pSi/Al Schottky diode presents the following parameters: n, I_0, ϕ_b and R_s are found to be 3.5, 32 nA, 0.74 V and 5.4 kΩ respectively. Under illumination of 150 watts, these values become 1.6, 1.1 nA, 0.9 V and 1.6 kΩ respectively as shown in figure 9.20. Electronic parameters of Al/ZnO/pSi/Al Schottky diode are gathered in table 9.5 in dark and light conditions.

TABLE 9.5
Ideality factor (n), saturation current (I_0), height barrier Φ_B and series resistance (R_s) and photoresponse of Al/ZnO/pSi/Al Schottky diode in dark and with several powers and temperatures [34]

Parameters of measurements ZnO SD		n	I_0 (nA)	Φ_B (V)	Rs by slope (kΩ)	Photo response
P (watts)	0	3.5	32	0.74	5.4	-
	60	1.9	42	0.79	2.1	1730
	90	1.5	16	0.89	2.8	1945
	120	1.1	2	0.86	1.4	3502
	150	1.6	1.1	0.90	1.6	3891
T (K)	295	3.02	34	0.74	2.5	-
	320	2.55	73	0.79	2.5	
	340	2.49	14	0.89	1.6	
	360	2.51	260	0.86	1.0	
	380	2.67	450	0.89	1.2	

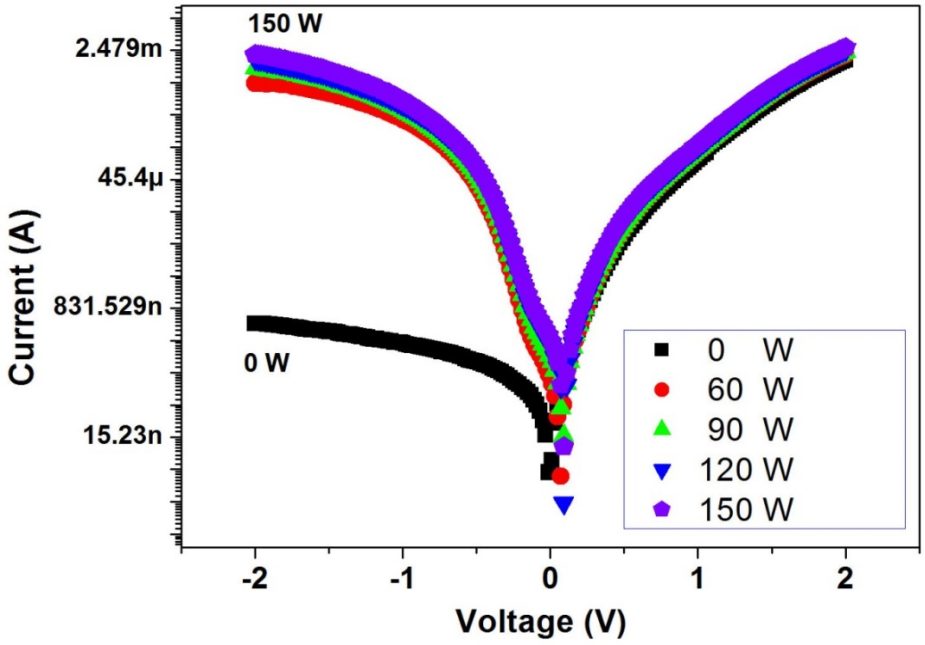

FIGURE 9.20
The semilog plot of the current-voltage characteristics of Al/ZnO/pSi/Al Schottky diode measured in dark and at several light powers at room temperature

Fabrication of thin films for sensors devices

In order to test the sensitivity of such oxide, we fabricate devices which own sensing properties like Sn doped In_2O_3 by e-beam evaporation [35]. The sensors conductance G is expressed by,

$$G = e\mu_n n\frac{S}{L} = e\mu_n \frac{S}{L}\ (n_o + \delta_n) \tag{4}$$

Where e and μ_n are the electron charge and mobility respectively, S and L are respectively the cross-sectional area and length of the sensing layer and n_o is the free electrons at the adsorption-desorption equilibrium. The sensitivity and transient response of the In_2O_3 sensor towards ethanol is found poor which can be improved by incorporating some suitable material over optimized In_2O_3.SnO_2 is one such material having sensitivity in the measurable range, stable microstructure and sensitive to gas response. For sensitizing reaction, reaction gas is observed with contact on the surface of the In_2O_3.SnO_2 film layer to form the Schottky contact and the electrical resistance of the sensor is changed.

$$O_{2\,(gas)} + 2e^- \longrightarrow 2O^- + \Delta H_1 \tag{5}$$

The detection reactions, participation of oxygen which can be in molecular (O_2) or in atomic (O^-) forms to reduce the resistance of the film.

$$C_2H_5OH_{\,(gas)} + O^- + \Delta H_2 \longrightarrow e^- + CH_3CHO_{(gas)} + H_2O + \Delta H_3 \tag{6}$$

On combining these two reactions mentioned above, the overall reaction on the surface can be given as,

$$O_{2\,(gas)} + 2C_2H_5OH_{\,(gas)} \longrightarrow 2CH_3CHO_{\,(gas)} + 2H_2O + \Delta H_4 \tag{7}$$

Sensitivity versus time of ITO films for 5, 10, 15, 20, 25min @ various SnO_2 amounts is displayed in figure 9.21 below.

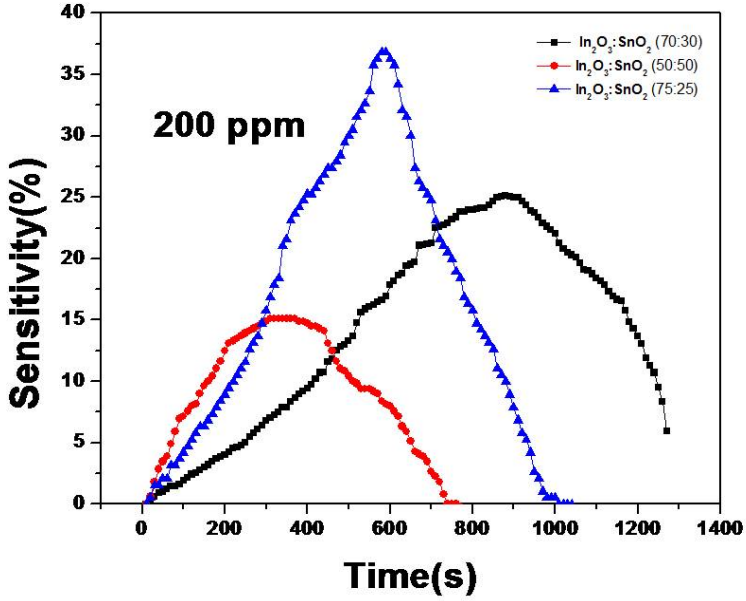

FIGURE 9.21
Sensitivity versus time of ITO films for 5, 10, 15, 20, 25min @ various SnO_2 amounts

Conclusions

Several semiconductor oxides in nanostructured thin films and devices have been proposed and investigated as basis devices for the solar cells fabrications. Metallic oxides have become as competitive material to GaN, GaAs, InSb and InP in electronic device fabrication and in optical, electronic and optoelectronic and sensing devices. This study provides a guidance on the selection of materials for optoelectronic device fabrications and on related physical, surface and electronic properties. Nanostructures of aluminium doped tin oxide sprayed onto ITO glass substrate are successfully synthesized. An (101)-oriented tetragonal crystalline structure is confirmed by X-ray patterns analysis. According to the (211) orientation the obtained grain size of the as-grown films obtained is lower. Thin films showed nanostructures with a size of 70 nm. Nanotips are also observed, growing from inner to the surface, having an average diameter of 180 nm respectively. The films' typical transmittance in the visible range is 85% and the optical bandgap is found to be 3.7 eV. Through this study, we report that the lowest resistivity of such oxide is lesser which is very good and competitive with other leading material candidates.

Nanostructured semiconductors of pure and indium-doped zinc oxide films have been obtained using a soft chemical spray pyrolysis method. Based on X-rays pattern, the wurtzite crystalline structure of as-synthesized films is confirmed. The IZO layers are polycrystalline and have grown according to (002) orientation. We observe that the lattice parameters are roughly altered by indium doping and the unit cell is slightly strained. An amount of dislocation occurs in IZO lattice ($0.002\ nm^{-2}$). A high visible and IR transparency around 88% is measured for IZO. Intense yellow (2.1 eV) and blue (2.8 eV) emissions are detected, and furthermore a weak green (2.3 eV) light is emitted from IZO nanostructures.

The DC sputtered p-type CuO thin films and Ag/CuO/nSi Schottky diode have been studied. The as-grown CuO film onto glass substrate is produced by sputtering. A (111)-oriented monoclinic crystalline structure is confirmed by XRD analysis. The films revealed a high transparency, around 80%, in both Vis and IR bands and optical band gap decreases from 2.52 to 1.99 eV when temperature increases. At high temperature of 550°C, the bulk concentration, the resistivity and mobility are of $46\times10^{17}\ cm^{-3}$, 22 Ω·cm and 0.06 cm^2/Vs. The extracted electronic parameters are deduced from I-V characteristics and are of : n = 3.5 , V_{oc}= 0.290 v, I_{sc}= 5.5 10^{-4} A, the obtained I_0 value is 2.3×10^{-8} A. the non-ideal behavior of as-fabricated diode is confirmed and caused by the series resistance (R_s) occurrence. By Norde method R_s is of 86.6 Ω and barrier height is around 0.96 V.

The gas sensing experiment shows good response from optimized indium oxide, 20 min tin oxide coating over optimized In_2O_3 film. Those films are more sensitive towards the 200 ppm of ethanol vapour. Consequently, ITO is a good candidate for sensor device fabrication.

Acknowledgements

Throughout the last four years, I have worked on exploiting chemical processes to fabricate and study the physical properties of various pure and doped oxide films. It has been a good opportunity for me to make a lot of samples which achieved with different deposition techniques and to gain experience on the role of a deposition technique and its competitiveness in producing novel materials. This work is included in project PNR 311/R77 entitled "PRODUCTION DES NANOSTRUCTURES A BASE DE SEMICONDUCTEUR D'OXYDE DE ZINC ET APPLICATION DANS LE

SOLAIRE" 2011-2013 financed by DGRSDT www.dgrsdt.dz and ATRST www.atrst.dz, and in CNEPRU project under number (B00L02UN310220130011) supported by Oran University of Sciences and Technology and MESRS www.mesrs.dz. I would like to thank everyone of my colleagues from Algerian, Turkish and Mexican universities for their support in this effort. The first author is grateful for the assistance of virtual library of SNDL https://www.sndl.cerist.dz. He would like to thank the assistance of DUBTAM center head, Dicle University- Diyarbakir Turkey, Prof. Dr . H. Temel, Dr. Y.S. Ocak, and Prof A. Tiburcio-Silver from Estado de Mexico, Mexico. I also would like to acknowledge the generous assistance and the effort of Prof. Dr. M.S. Aida (Thin Films & Plasma Lab., Physics Department, Mentouri University, Constantine, Algeria). The first author thanks Prof. Dr. A. Sanchez Juarez (Centro de Investigacion en Energia CIE-UNAM, Temixco, Morelos Mexico) and Dr. Z. Mouffak (Department of Electrical and Computer Engineering, California State University, Fresno, CA, USA) for their contributions.

References

1. Benouis C E, Benhaliliba M, Mouffak Z, Avila-Garcia A, Tiburcio-Silver A, Ortega Lopez M, Romano Trujillo R, Ocak Y S. The low resistive and transparent Al-doped SnO_2 films: p-type conductivity, nanostructures and photoluminescence. Journal of Alloys and Compounds. 2014; 603: 213-223.
2. Benhaliliba M, Benouis C E, Tiburcio-Silver A, Yakuphanoglu F, Avila-García A, Tavira A, Trujillo R R, Mouffak Z. Luminescence and physical properties of copper doped CdO derived nanostructures. Journal of Luminescence. 2012; 132 (10):2653-2658.
3. Vaishnav V S, Patel S G, Panchal J N. Development of ITO thin film sensor for detection of benzene. Sensors and Actuators B 2015; 206 :381–388.
4. Sethupathi N , Thirunavukkarasu P, Vidhya V S, Thangamuthu R, Kiruthika G V M, Perumal K, Bajaj Hari C , Jayachandran M. Deposition and optoelectronic properties of ITO (In_2 O_3 :Sn) thin films by Jet nebulizer spray (JNS) pyrolysis technique. J Mater Sci: Mater Electron. 2012; 23:1087–1093.
5. Benhaliliba M, Benouis C E, Boubaker K, Amlouk M, Amlouk A. A New Guide to Thermally Optimized Doped Oxides Monolayer Spray-Grown Solar Cells: The Amlouk-Boubaker Optothermal Expansivity ψ_{AB}. Edited by Leonid A. Kosyachenko, Publisher: InTech, pp. 27–41, 2011. www.intechweb.org, (2011) DOI: 10.5772/21046, "Solar Cells - New Aspects and Solutions", book edited by Leonid A. Kosyachenko, ISBN 978-953-307-761-1.
6. Ganesh T, Rajesh S, Xavier F P. Effect of Al dopant concentration on structural, optical and photoconducting properties in nanostructured zinc oxide thin films. Materials Science in Semiconductor Processing.2013; 16 (2): 295-302.
7. Aydın C, Benhaliliba M, Al-Ghamdi Ahmed A, Gafer Zarah H, El-Tantawy, Yakuphanoglu F. Determination of optical band gap of ZnO:ZnAl2O4 composite semiconductor nanopowder materials by optical reflectance method. Journal of Electroceramics. 2013 ; 31 : 265-270.
8. Zhong W W, Liu F M, Cai L G , Zhou C C , Ding P, Zhang H. Annealing effects of co-doping with Al and Sb on structure and optical–electrical properties of the ZnO thin films. Journal of Alloys and Compounds. 2010 ; 499 : 265–268.
9. Caglar M, Ilican S, Caglar Y, Yakuphanoglu F. The effects of Al doping on the optical constants of ZnO thin films prepared by spray pyrolysis method. J Mater Sci: Mater Electron. 2008 ; 19:704–708.

10. Ozturk S, Kilinç N¸ Torun I, Kosemen A, Sahin Y, Ziya Ozturk Z. Hydrogen sensing properties of ZnO nanorods: Effects of annealing, temperature and electrode Structure. International Journal of Hydrogen Energy. 2014; 39: 5194 -5201.
11. Tombak A, Benhaliliba M, Ocak Y S, Kiliçoglu T.The novel transparent sputtered p-type CuO thin films and Ag/p-CuO/n-Si Schottky diode applications. Results in Physics. 2015 ; 5 :314-321.
12. Zeng Wen, Tianmo Liu, Zhong Chang Wang, Physica. Sensitivity improvement of TiO_2-doped SnO_2 to volatile organic compounds. 2010 ; 43 :633-638.
13. Pietruszka R , Witkowski B S, Gieraltowska S, Caban P, Wachnicki L, Zielony E, Gwozdz K, Bieganski P, Placzek-Popko E, Godlewski M. New efficient solar cell structures based on zinc oxide nanorods. Solar Energy Materials and Solar Cells**.** 2015; 143: 99-104.
14. Tsai, Chih-Hung , Chih-Han Chen, Po-Hsi Fei, Yu-Kuei Hsu. Novel Semiconductor-Liquid Heterojunction Solar Cells Based on Cuprous Oxide and Iodine Electrolyte. Electrochimica Acta. 2015 ; 167 : 112–118.
15. Korotcenkov G , Brinzari V, Gulina L B, Cho B K . The influence of gold nanoparticles on the conductivity response of SnO_2-based thin film gas sensors. Applied Surface Science**.** 2015; 353: 793–803.
16. Lin Tzu-Shun , Ching-Ting Lee. Homostructured ZnO-based metal-oxide-semiconductor field-effect transistors deposited at low temperature by vapor cooling condensation system. Applied Surface Science. 2015**,** 354:71-73.
17. Husairi F S, Rouhi J, Eswar K A, Raymond Ooi C H, Rusop M, Abdullah S. Ethanol solution sensor based on ZnO/pSi nanostructures synthesized by catalytic immersion method at different molar ratio concentrations: An electrochemical impedance analysis. Sensors and Actuators A: Physical. 2016; 236: 11–18.
18. Suriani A B , Dalila A R, Mohamed A, Mamat M H, Malek M F , Soga T, Tanemura M. Fabrication of vertically aligned carbon nanotubes–zinc oxide nanocomposites and their field electron emission enhancement. Materials & Design. 2016; 90 (15):185–195.
19. Suman P H, Felix A A, Tuller H L, Varela J A, Orlandi M O. Comparative gas sensor response of SnO_2, SnO and Sn_3O_4 nanobelts to NO_2 and potential interferents. Sensors and Actuators B: Chemical**.** 2015; 208:122–127.
20. Ridong C, Wang Q, Zhang J, Wang J, Xu Y, Jin Y, Cui Q. Plasma-assisted synthesis of zinc nanowires. Materials Chemistry and Physics. 2011; 129: 611-613.
21. Ahmed Sk. F., P.K. Ghosh, S. Khan, M. K. Mitra, K.K. Chattopadhyay. Low-macroscopic field emission from nanocrystalline Al doped SnO_2 thin films synthesized by sol–gel technique. Appl.Phys. 2007;A 86:139-143.
22. Benhaliliba M, Benouis C E, Yakuphanoglu F, Tiburcio-Silver A, Aydin C, Hamzaoui S, Mouffak Z. Detailed investigation of submicrometer-sized grains of chemically sprayed(Sn1−xAlx, O2) (0≤x≤0.085) thin films. Journal of Alloys and Compounds. 2012; 527:40-47.
23. De Moure-Flores F, Quiñones-Galván J G, Hernández-Hernández A, Guillén-Cervantes A, Santana-Aranda M A, de la L. Olvera M, Meléndez-Lira M. Structural, optical and electrical properties of Cd-doped SnO_2thin films grown by RF reactive magnetron co-sputtering. Appl. Surf. Sci. 2012 ; 258 :2459–2463.
24. Chacko, S., N.S. Philip, K.G. Gopchandran, P. Koshy, V.K. Vaidyan. Nanostructural and surface morphological evolution of chemically sprayed SnO 2 thin films. Appl. Surf. Sci. 2008; 254:2179-2186.

25. Benhaliliba M, Benouis C E, Mouffak Z, Ocak Y S, Tiburcio-Silver A, Aida M S, Garcia A A, Tavira A and Sanchez Juarez A. Preparation and Characterization of Nanostructures of In-Doped ZnO films Deposited by Chemically Spray Pyrolysis: Effect of Substrate Temperatures. Superlattices and Microstructures, 2013; 63: 228-239.
26. Zhang, L.D., C.M. Mo. Luminescence in nanostructured materials. J. Nano-Struct. Mater. 1995; 6 :831–840.
27. Ji T H, Liu Y, Zhao H, Du H, Sun J, Ge G. Preparation and up-conversion fluorescence of rare earth (Er^{3+}or Yb^{3+}/Er^{3+})-doped TiO_2 nanobelts. J. Solid State Chem. 2010; 183 : 584–589.
28. Ningning Yan, Zhongqi Zhu, Jin Zhang, Zongyan Zhao, Qingju Liu. Preparation and properties of ce-doped TiO_2 photocatalyst. Materials Research Bulletin. 2012; 47:1869-1873.
29. Sun C, Li H, Zhang H, Wang Z, Chen L. Controlled synthesis of CeO_2 nanorods by a solvothermal method. Nanotechnology, 2005; 16: 1454–1463.
30. Paine D C , Whiston T, Janiac D , Bersford R , Yang C O , Lewis B. A study of low temperature crystallization of amorphous thin film indium–tin–oxide. J. Appl. Phys. 1999; 85 : 8445.
31. Sze S M, Ng K K. Physics of Semiconductor Devices. 2007; Third ed. (John Wiley & Sons: New Jersey).
32. Missoum I, Benhaliliba M, Chaker A, Ocak Y S, Benouis CE. A Novel device behavior of Ag/MgPc/n-GaAs/Au-Ge organic based Schottky Diode.Synthetic Metals. 2015; 207: 42–45.
33. Norde H J. A modified forward IV plot for Schottky diodes with high series resistance Appl. Phys. 1979 ; 50 : 5052.
34. Benhaliliba M, Ocak Y S, Mokhtari H, Benouis C E, Aida M S. The microelectronic parameters of Al /ZnO/p-Si/Al Schottky diode for solar cell applications. DUFED 2015; 4(1): 55-58.
35. Ayeshamariam A, Bououdina M, Sanjeeviraja C. Optical, electrical and sensing properties of In_2O_3 nanoparticles. Materials Science in Semiconductor Processing, 2013; 3: 686–695.